MODIFICATION OF HIGH-SPEED STEELS BY NITROGEN COMPRESSION PLASMA FLOW: STRUCTURE, ELEMENT COMPOSITION, TRIBOLOGICAL PROPERTIES.

N. N. Cherenda*[1], V.V. Uglov[1], V.M. Anishchik[1], A.K. Stalmashonak[1], V.M. Astashinski[2], G. Thorwath[3], B. Stritzker[3].

[1]Belarusian State University, F. Scorina 4, 220080 Minsk, Belarus.

[2]Institute of Molecular and Atomic Physics of the National Academy of Sciences of Belarus, F. Scorina 70, 220072 Minsk, Belarus.

[3]Institut für Physik, Universität Augsburg, Lehrstuhl für Experimentalphysik IV, Universitätsstrasse 1, D-86135 Augsburg, Germany

The influence of the nitrogen compression plasma flow impact on the phase and element composition, tribological properties of AISI M2 and AISI T1 high-speed steels was investigated in this work. The bank capacitor initial voltage, the number of pulses and nitrogen pressure in the vacuum chamber varied during experiments providing the change of energy deposited in the surface layer within the limits of 5–13 J/cm^2 per pulse. It was found that treatment resulted in carbides partial dissolution and austenite formation in the surface layer. The modified layer thickness amounted to 24 μm while the nitrogen penetration depth did not exceed 400 nm. Treatment by the compression plasma flow mainly led to the decrease of hardness and the friction coefficient of high-speed steels.

Keywords: high-speed steel, plasma flow, structure-phase transformation.

---

*Corresponding author: Tel.: +375 17 2265834; Fax: +375 17 2095445,

E-mail: cherenda@bsu.by

1. Introduction

Different types of ion-plasma nitriding techniques are used for modification of steels mechanical properties [1-9]. Some techniques, e.g. plasma immersion ion implantation, find their application in industry. A comparatively short treatment time (a few tens of minutes – a few hours) is the main advantage of these methods in comparison with convenient nitriding. The use of techniques based on the direct interaction of high temperature plasma with a material allows to decrease even this period [10-12]. Direct dense plasma flows with small divergence and high energy (up to 30 J/cm^2) can modify a layer with thickness of tens of micrometers in an extremely short time < 1 second. Treatment of low-alloyed steels by different types of direct plasma flows resulted in a substantial increase of their mechanical properties [11, 12].

The investigation of the effect of the nitrogen compression plasma flow (CPF) impact on the structure and tribological properties of high-speed steels was the aim of this work. Improved tribological properties of high-speed steels are usually achieved by complicated metallurgical thermal treatment. At the same time high temperature, high cooling speed in the surface layer of steel during CPF treatment can result in the change of carbide morphology, concentration of residual austenite, the microstructure of martensine grains causing a possible worsening of tribological properties (while nitrides formation improves it). It means that CPF treatment of a high-speed steel could cause tribological properties improvement in a narrow range of treatment parameters only. That is why it is necessary to study the influence of CPF treatment parameters (the energy of a discharge capacitor, nitrogen pressure in a vacuum chamber, the number of pulses) on the phase and elemental composition, microstructure and tribological properties of high-speed steels.

2. Experimental

The effect of CPF treatment on two high-speed steels AISI M2 and AISI T1 was investigated in this work. Samples of AISI M2 steel had the following element composition: 0.8% C, 6.0% W, 5.0% Mo, 4.1% Cr, 1.9% V, 0.5% Co in wt. %. The element composition of AISI T1 samples was the following: 0.8% C, 18.7% W, 4.3% Cr, 1.9% V, in wt.%. T1 steel possesses higher thermal stability than M2 steel due to higher tungsten content. The steel samples were subjected to thermal processing, which is typical of this type of steel. The phase composition of the samples includes the following main phases: α-Fe doped with alloying elements, M_6C, MC and $M_{23}C_6$ carbides (M: Fe, W, Cr, Mo, V).

The gas discharge magnetoplasma compressor used for generating CPF was described in details in [13]. The experiments were performed in a 'residual gas' mode during which the vacuum chamber was filled with nitrogen. The pulse duration was 100 μs. Three types of experiments were carried out to study the influence of the treatment parameters on steels structure and properties.

The first type of experiments: the influence of the number of pulses (n) was investigated using M2 steel samples. This experiment was carried out at the nitrogen pressure of 0.4 kPa. The number of pulses was 1 and 5 at the bank capacitor initial voltage (U_0) - 4 kV. According to the calorimetric measurements the value of the power density absorbed by the sample surface (Q) was approximately 13 J/cm^2 per pulse.

The second type of experiments: the influence of the bank capacitor initial voltage was also investigated using M2 steel samples. The value of the nitrogen pressure in the vacuum chamber was the same - 0.4 kPa. U_0 was equal to 2.9 kV and 3.6 kV at one pulse. The value of the power density absorbed by the sample surface was approximately 5 J/cm^2 for U_0=2.9 kV and 10 J/cm^2 for U_0=3.6 kV

The third type of experiments: the influence of the nitrogen pressure (P) in the vacuum chamber was investigated using T1 samples. The nitrogen pressure varied in the range of 0.4 - 4.0 kPa in these experiments. The bank capacitor initial voltage was 3 kV, the number of pulses was 1 and 5.

The phase composition of the samples was investigated using X-ray diffraction analysis (XRD) in the Bragg- Brentano geometry, with a Cu Kα radiation. The calculated X-ray penetration depth in iron was 0.7-1.2 μm for $2\theta=30^o$-50^o assuming the absorption of 75% of X-ray energy. The concentration profiles of elements were measured by Auger electron spectroscopy (AES) using PHI-660 (Perkin Elmer). Rutherford backscattering analysis (RBS) of He ions with the energy of 6 MeV was also used for the determination of the nitrogen atoms penetration depth. High energy of helium ions allows to increase the yield of ions scattered on light impurities. Surface and cross-section morphology was studied by scanning electron microscopy (SEM) and optical microscopy (OM). Microhardness of the samples was tested by means of a PMT-3 microhardmeter with a Vickers indentor under the load ranging from 1 to 2 N. The tribological test was of the 'pin-on-plane' type, dry sliding dynamic friction. The linear velocity was 0.4 cm/s. The pin was made of a hard alloy (92 wt.% WC, 8 wt.% Co). The load on the pin was 0.7 N for M2 steel and 1 N for T1 steel.

3. Results and discussion

3.1. AISI M2 steel

The results of the M2 steel phase composition analysis before and after treatment are presented in Fig. 1 and Fig. 2. One can see that the diffraction pattern of M2 steel in the initial state (Fig. 1) contains diffraction lines of α-Fe, M_6C and MC – the main carbides in high-speed steels. Treatment even with one pulse of CPF at U_0=4kV (Q=13 J/cm^2) has resulted in dissolution of M_6C and MC carbides in the analyzed layer (Fig. 1). This indicates that the temperature of the surface layer was at least greater a 1573 K - the temperature of M_6C dissolution. MC carbide is considered insoluble in high-speed steels, while in steels containing only vanadium it dissolves at the temperature of 1373 K. Heating to these temperatures may result in austenite formation. One can see the presence of austenite diffraction lines after treatment with one pulse (Fig. 1). At room temperature the existence of the γ-Fe phase can be stabilized by nitrogen incorporated into the f.c.c. lattice. A similar effect can be obtained by incorporation of Cr which is in steel, into the f.c.c. lattice. The (111) γ-Fe diffraction line is shifted into the area of smaller 2θ angles as in case of expanded nitrogenous austenite formation [14]. Expanded austenite is usually observed after nitriding austenite stainless steels with a high Cr concentration [6, 14]. A significant shift of the (200) γ-Fe diffraction line is also typical of expanded austenite [14] because nitrogen should mainly be located in octahedral pores of the f.c.c. lattice [15]. In our case the position of the (200) γ-Fe diffraction line corresponds well to standard data. The shift of the (111) γ-Fe line and lattice distortion can be mainly connected with incorporation of W, Cr, Mo and V atoms from dissolved carbides into the iron f.c.c. lattice. Thus, according to the obtained diffraction patterns the formation of the γ-Fe phase doped with C, N, Cr, W, Mo and V can be assumed. The increase of n led to the growth of the austenite diffraction line intensity, i.e. the growth of austenite content in the analyzed layer.

The main reason for the observed effects is energy deposited in the surface layer during the CPF impact. The diminishing of U_0 up to 2.9 kV (Q=5 J/cm^2) during treatment almost did not change the phase composition of M2 steel (Fig. 2). While the treatment at U_0=3.6 kV (Q=10 J/cm^2) resulted again in austenite formation, MC and M_6C carbides dissolution. It should be noted that no evidence of nitrides formation was found during the phase analysis.

The influence of high temperature on the surface during CPF is well seen in the Fig. 3. The grinding traces observed on the surface of the initial sample (Fig 3a) disappeared after CPF treatment (Fig. 3b). One can see the flowed surface even at the lowest value of U_0 used in the experiments.

Morphology of the modified layer cross-section was investigated using OM and SEM. The cross-section of M2 steel samples before and after CPF treatment with a different number of pulses at U_0=4 kV is presented in Fig. 4. One can see that the thickness of the modified layer (a white layer) increases with the growth of n. It amounts to ~ 18 μm at one pulse (Fig 4b) and to 24 μm at 5 pulses (Fig 4c). The structure of the modified layer allows to conclude that it contains austenite. It is in agreement with the XRD data (Fig. 1). But the thickness of the austenite containing layer appears significantly greater than the XRD analyzing depth. It means that the temperature of the near surface layer with the thickness ~ 20 μm is greater than the temperature of α→γ transformation during treatment. The real temperature of the surface layer can be considerably greater – up to 2000-3500 K [16, 17]. Austenite should be stabilized by some type of impurity at the whole depth of the modified layer. That is why either nitrogen or chromium atoms incorporation into the f.c.c. lattice can be supposed in the layer with the thickness of ~ 20 μm.

Morphology of the cross-section of M2 steel treated at different U_0 is shown in Fig. 5. In case of CPF treatment at U_0=2.9 kV the thickness of the modified layer is approximately 8-9 μm (Fig. 5a). This layer contains M_6C carbides of a smaller size than those in the bulk of the layer. The increase of U_0 resulted in the growth of the modified layer thickness up to 12 μm (Fig. 5b). This layer can be divided into two main sublayers. A similar structure of the modified layer is observed in Fig. 4b (U_0=4 kV). The first sublayer with the thickness ~ 6 μm contains austenite and small inclusions of MC carbide (Fig. 5c). This sublayer includes the surface layer with the thickness of ~ 1 μm (X-rays analyzing depth) containing no carbides at all. These data are also in agreement with those of the phase analysis (Fig. 2). The size of MC carbide increases with the depth. No M_6C carbides were found in this sublayer. Small M_6C carbides appeared only in the second sublayer with the thickness of ~ 6 μm.

Though no change of the phase composition was found in the M2 sample treated at U_0=2.9 kV carbide dissolution took place even at this treatment regime. The cross-section of this sample is presented in Fig. 6. The element composition at the points indicated in Fig. 6 is summarized in the Table. Points 1 and 2 correspond to M_6C carbide. The concentration of alloying elements in carbide is greater in the depth of the sample where the temperature during treatment should be less. The change of Cr concentration lies in the limits of measurement inaccuracy. These data show that the alloying elements begin to diffuse into the iron matrix from carbide in the surface layer during treatment.

It was found that the growth of energy deposited in the surface layer either by the increase of U_0 or by the n increase led to the growth of the modified layer thickness. The deposited energy also influenced the phase composition (carbide presence) in the modified layer.

M_6C and MC carbides disappeared at Q=10 J/cm^2. Austenite formation was found almost at all treatment regimes used except of U_0=2.9 kV.

The observed changes in the phase composition of M2 steel strongly influence its tribological properties (Fig. 7). The growth of energy deposited in the surface layer led to the microhardness decrease due to hardening carbides dissolution (Fig. 7a and Fig 7b). Only the sample treated with the lowest voltage used U_0=2.9 kV possesses the same or slightly greater value of microhardness in comparison with the initial one (Fig. 7b). For all treatment regimes improvement in the friction coefficient behaviour is observed (Fig. 7c and Fig. 7d). A slight increase of the friction coefficient takes place at the initial stage of friction. However, 2.5 times decrease of the friction coefficient is observed during at the stage of steady-state friction. Wear track were not seen visually on the surface in contrast to the origin sample. This indicates small wear in the treated samples. All treated samples possess approximately equal friction coefficient of ~ 0.15-0.2 in spite of different hardness (different hardening carbide content) of the surface layer. Thus, it can be assumed that the main reason for friction coefficient improvement should be the same. It is known that nitrogenous austenite has high wear-resistance [18]. The formation of nitrogenous austenite was clearly observed after CPF treatment (Fig. 1 and 2) except of the sample treated at U_0=2.9 kV (Fig. 2). In the last case austenite formation should be also expected because the temperature of the surface layer was near or greater than the melting temperature (Fig. 3). A thin austenite layer can give a very small diffraction line (111)γ-Fe which cannot be resolved at the diffraction pattern due to the presence of (200)MC diffraction line almost at the same position. That is why the friction coefficient decrease can be explained most likely by the formation of nitrogenous austenite in the surface layer, though the change of surface roughness can also influence the friction coefficient value.

3.2. AISI T1 steel

The AES depth profiles of nitrogen atoms in treated T1 steel are shown in Fig. 8. All nitrogen depth profiles exhibit a well-known system of a near surface compound layer containing nitrides and a deeper diffusion layer obtained after nitrogen treatment [8, 19]. Nitrogen distributions have a similar character but strongly differ in the penetration depth. Besides that the surface nitrogen concentration in the sample treated at P=2.7 kPa and n=1 differs from the surface nitrogen concentration in other samples. This feature is connected with the presence of a contaminating carbon layer on the surface and the following normalization of atomic concentration to 100 %. The growth of the nitrogen pressure in the vacuum chamber (in the range of 0.4-2.7 kPa) resulted in the increase of nitrogen content in the modified layer and in the

increase of the nitrogen penetration depth. The growth of the pulse number at P=2.7 kPa also led to the increase of nitrogen content in the modified layer. The maximum concentration of nitrogen (33 at.%) is observed in the sample treated at P=2.7 kPa and n=5. A further increase of P can result in the decrease of nitrogen content because the excess of nitrogen atoms in the vacuum chamber will be an obstacle for plasma flow spreading. The nonlinear dependence of the nitrogen concentration on the pressure of nitrogen was already observed during laser nitriding austenitic stainless steel [20].

RBS investigations were carried out to determine nitrogen penetration depth. Nitrogen AES and RBS depth profiles in T1 steel treated by CPF at U_0=3 kV, P=2.7 kPa and n=5 are shown in Fig. 9. One can see that the results of these two techniques are in agreement with each other. The maximum nitrogen penetration depth is about 350-400 nm. This value is significantly smaller than the thickness of the modified layer observed in M2 steel (Fig. 4 and Fig. 5). The phase and element composition of M2 and T1 is quite similar except of Mo and W content. Greater tungsten content in T1 steel can slightly decrease the nitrogen diffusion depth but the order of the penetration depth will be just the same. That is why one can expect a similar nitrogen penetration depth in M2 steel. So the presence of austenite in the modified layer of M2 steel (Fig. 4) is mainly connected with the incorporation of chromium atoms into the f.c.c. lattice. Free chromium atoms necessary for austenite stabilization can appear during dissolution of carbides, in particular chromium rich $M_{23}C_6$.

The findings showed that CPF treatment also resulted in tungsten redistribution in the surface layer with the thickness of 1 μm (Fig. 10). Tungsten segregation with the concentration of 8 at. % is observed at the depth of 200 nm in the initial state. The concentration in the segregation maximum diminishes with the growth of energy deposited in the surface layer during treatment. At P=2.7 kPa and n=5 this concentration is equal to tungsten concentration in the bulk of the sample – 6 at. %. Diffusion of nitrogen and tungsten atoms occurred due to a high temperature gradient during treatment.

The phase composition was investigated in the T1 sample containing the maximum quantity of nitrogen (Fig. 11). The diffraction lines of hardening carbides M_6C, MC and $M_{23}C_6$ are well seen on the diffraction pattern before treatment. CPF treatment resulted in partial dissolution of carbides and austenite formation as in case of M2 steel. At the same time a weak line of ε-$Fe_{2+x}N$ or ε-Fe_{2+}x(N, C) was found at the diffraction pattern (Fig. 11). Same nitride or carbonitride was found during plasma immersion implantation of ferritic steels [7, 9]. The nitrogen concentration in a thin compound layer (Fig. 8) lies in the limits of the nitride stoichiometry change. Therefore, in spite of a relatively high concentration of nitrogen in the surface layer only a small part of nitrogen atoms took part in nitride formation. The

concentration of nitrogen in austenite can be as much as 12 at. % [20]. That is why nitride formation can be expected in the thin surface compound layer and in the diffusion zone in which nitrogen concentration exceeds this value. At the same time the presence of alloying elements in the f.c.c. lattice can change the limit of nitrogen content in austenite. The total depth of the layer that can contain nitride precipitates is ~ 100 nm (Fig. 8). In a deeper layer nitrogen atoms will be incorporated into austenite.

The change of the nitrogen pressure in a vacuum chamber during treatment strongly affects hardness of samples (Fig. 12a). The maximum hardness decrease is observed in the sample treated at P=2.7 kPa and n=5. According to the results of the M2 and T1 samples phase analysis this sample can contain the minimum volume fraction of hardening carbides in the surface layer. One can see that the hardness dependence on the nitrogen pressure has a nonlinear character. It means that the increase of P up to 4 kPa weakens the effect of compression plasma flow on samples. At the same time CPF treatment positively affects the friction coefficient of T1 steel (Fig. 12b) resulting in its decrease. The friction coefficient dependences of the samples treated at P=0.4 kPa and P=4 kPa are equal to the friction coefficient dependence of an untreated sample. The increase of the friction coefficient at the initial stage of friction is observed as in case of M2 steel. It can be connected with the presence of a thin brittle compound layer destroyed during friction with the formation of hard wear particles [21]. A different load on a friction pair conditions a difference in a type of dependence for M2 and T1 steels.

4. Conclusions

Nitrogen CPF treatment resulted in a substantial modification of the initial structure of high-speed steels. Dissolution or partial dissolution of carbides and formation of austenite doped with nitrogen and alloyed elements were observed. The carbide dissolution rate and the austenite volume fraction are closely connected with the amount of energy deposited in the surface layer. The deposited energy growth led to the increase of the modified layer thickness which can be as much as 24 μm. The findings showed that most of nitrogen atoms were incorporated into austenite formed during treatment. The ε- phase observed during CPF treatment regimes providing the maximum content of nitrogen in the modified layer is formed probably in a thin surface layer where nitrogen concentration is greater than the limit of nitrogen content in austenite.

It was found that the nitrogen penetration depth depended on the nitrogen pressure in the vacuum chamber and the number of pulses. The maximum concentration of nitrogen on the surface amounted to 32 at. % and the maximum penetration depth to ~ 400 nm. The growth of

energy deposited in the surface layer of T1 steel resulted in the decrease of tungsten surface segregation and tungsten redistribution to the bulk of the sample.

Dissolution of carbides in the surface layer of high-speed steels led to the microhardness decrease. For M2 steel the treatment regime providing a slight increase of the microhardness value was found. At the same time CPF treatment allows to diminish the friction coefficient of a high-speed steel 2.5 times. Improvement in the friction coefficient behaviour was observed almost for all treatment regimes used.

Acknowledgements

This work was supported by the INTAS grant YSF 03-55-1345.

References

1. F. Borgioli, E. Galvanetto, A. Fossati, T. Bacci. Surf. Coat. Technol. 162 (2002) 61.
2. G.A. Collins, R. Hutchings, K.T. Short, J. Tendys. Surf. Coat. Technol. 103-104 (1998) 212.
3. Jerzy Robert Sobiecki, Pawel Mankowski, Aleksy Patejuk. Vacuum 76 (2004) 57.
4. S.K. Kim, J.S. Yoo, J.M. Priest, M.P. Fewell. Surf. Coat. Technol. 163 –164 (2003) 380.
5. H. Ferkel, M. Glatzer, Y. Estrin, R.Z. Valiev, C. Blawert, B.L. Mordike. Mater. Sci. Eng. A348 (2003) 100.
6. LiangWang, Xiaolei Xu, Zhiwei Yu, Zukun Hei. Surf. Coat. Technol. 124 (2000) 93.
7. G. Thorwarth, S. Mändl, B. Rauschenbach. Surf. Coat. Technol. 125 (2000) 94.
8. S. Mändl, E. Richter, R. Günzel, W. Möller. Nucl. Instr. and Meth. B 148 (1999) 846.
9. V.V. Uglov, J.A. Fedotova, A.K. Kuleshov, A.L. Danilyuk, N.T. Kvasov, R. Günzel, R. Reuther, E. Richter. Surf. Coat. Technol. 136 (2001) 226.
10. B.A. Kalin, V.L. Yakushin, V.I. Vasiliev, S.S. Tserevitinov. Surf. Coat. Technol. 96 (1997) 110.
11. I.E. Garkusha, O.V. Byrka, V.V. Chebotarev, N.T. Derepovski, G. Müller, G. Schumacher, N.S. Poltavtsev, V.I. Tereshin. Vacuum 58 (2000) 195.
12. V.M. Anishchik, V.V. Uglov, V.V. Astashynski, V.M. Astashynski, S.I. Ananin, E.A. Kostyukevich, A.M. Kuzmitski, N.T. Kvasov, A.L. Danilyuk, I.N. Rumianceva. Vacuum 70 (2003) 269.
13. V.V. Uglov, V.M. Anishchik, V.V. Astashynski, V.M. Astashynski, S.I. Ananin,V.V. Askerko, E.A. Kostyukevich, A.M. Kuz'mitski, N.T. Kvasov, A.L. Danilyuk. Surf. Coat. Technol. 158 –159 (2000) 273.
14. Orhan Ozturk, D.L. Williamson. Surf. Coat. Technol. 158 –159 (2002) 288.
15. Xiaolei Xu, Zhiwei Yu, Liang Wang, Jianbing Qiang, Zukun Hei. Surf. Coat. Technol. 162 (2003) 242.
16. A. Lepone, H. Kelly, D. Lamas, A. Marquez. Appl. Surf. Sci. 143 (1999) 124.
17. G.E. Remnev, I.F. Isakov, M.S. Opekounov, V.M. Matvienko, V.A. Ryzhkov, V.K. Struts, I.I. Grushin, A.N. Zakoutayev, A.V. Potyomkin, V.A. Tarbokov, A.N. Pushkaryov, V.L. Kutuzov, M.Yu. Ovsyannikov. Surf. Coat. Technol. 114 (1999) 206.
18. J. Langner, J. Piekoszewski, Z. Werner, V.I. Tereshin, V.V. Chebotarev, I. Garkusha, L. Walis, B. Sartowska, W. Starosta, W. Szymczyk, M. Kopcewicz, A. Grabias. Surf. Coat. Technol. 128-129 (2000) 105.
19. A. da Silva Rocha, T. Strohaecker, V. Tomala, T. Hirsch. Surf. Coat. Technol. 115 (1999) 24.
20. Han M., Landry F., Lieb K.-P., Schaaf P. Appl. Phys. A 69 (1999) S795.
21. B. Podgornik, J. Vizintin, V. Leskovsek. Wear 232 (1999) 231.

Table

The elements concentration (in wt. %) at points indicated in Fig. 6.

Point #	Cr	V	W	Mo	Fe
1	4.0	2.9	21.0	12.4	59.7
2	3.8	3.8	31.3	21.3	39.8

Figure captions

Fig. 1 XRD patterns of M2 steel before and after CPF treatment at U_0=4.0kV with a different number of pulses.

Fig. 2 XRD patterns of M2 steel and after one pulse of CPF treatment at U_0=2.9 kV and U_0=3.6 kV.

Fig. 3 SEM images of M2 steel before (a) and after CPF treatment at U_0=2.9 kV and n=1 (b).

Fig. 4 OM images of M2 steel cross-section before (a) and after CPF treatment at U_0=4.0 kV, n=1 (b) and at U_0=4.0 kV, n=5 (c).

Fig. 5 SEM images of M2 steel cross-section after one pulse of CPF treatment at U_0=2.9 kV (a) and at U_0=3.6 kV (b, c).

Fig. 6 SEM image of M2 steel cross-section after one pulse of CPF treatment at U_0=2.9 kV.

Fig. 7 Hardness (a, b) and friction coefficient (c, d) of M2 steel after CPF treatment at U_0=4.0kV with different number of pulses (a, c) and after one pulse of CPF treatment at U_0=2.9 kV and U_0=3.6 kV (b, d).

Fig. 8 Nitrogen AES depth profiles in T1 steel treated by CPF at different regimes.

Fig. 9 Nitrogen AES and RBS depth profile in T1 steel treated by CPF at U_0=3 kV, P=2.7 kPa and n=5.

Fig. 10 Tungsten RBS depth profiles in T1 steel before and after treatment by CPF at U_0=3 kV, P=2.7 kPa and different number of pulses.

Fig. 11 XRD patterns of T1 steel before and after CPF treatment (U_0=3 kV, P=2.7 kPa, n=5).

Fig. 12 Hardness (a) and friction coefficient (b) of T1 steel after CPF treatment at different regimes.

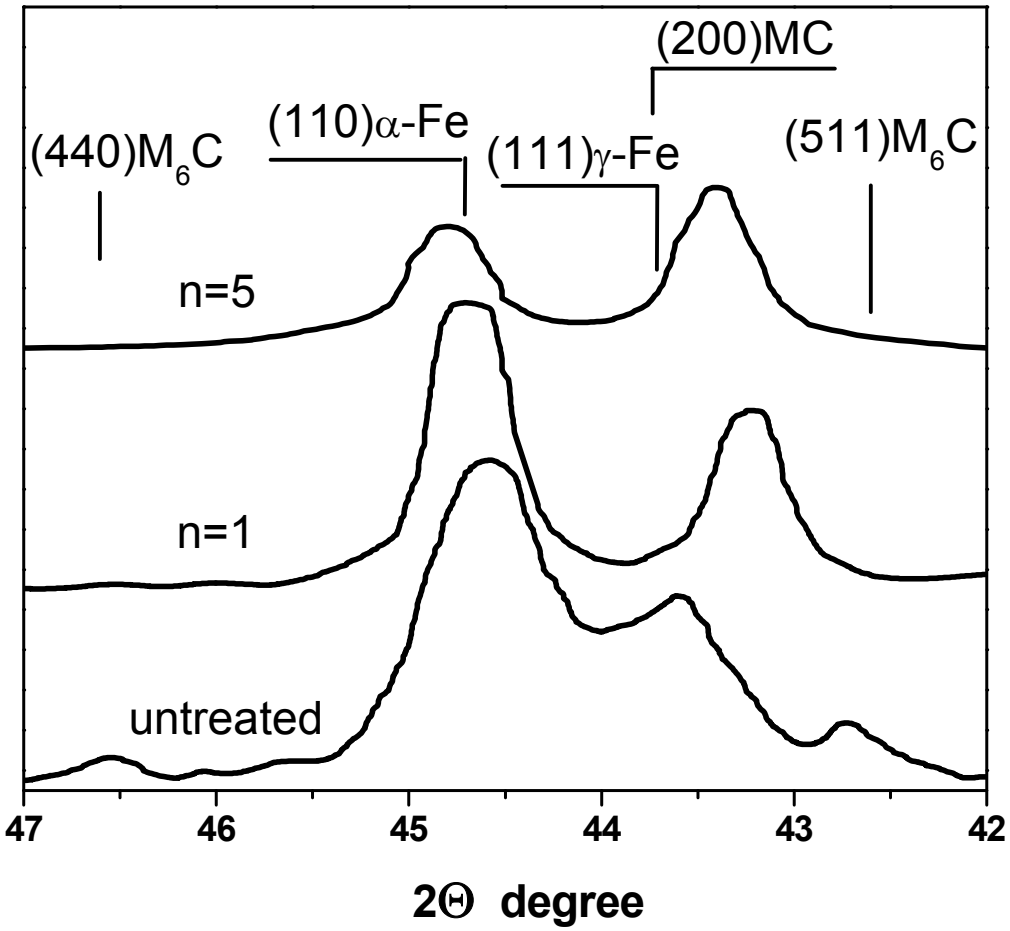
(200)MC
(110)α-Fe
(111)γ-Fe
(440)M6C
(511)M6C
n=5
n=1
untreated
47
46
45
44
43
42
2Θ degree

Fig. 1

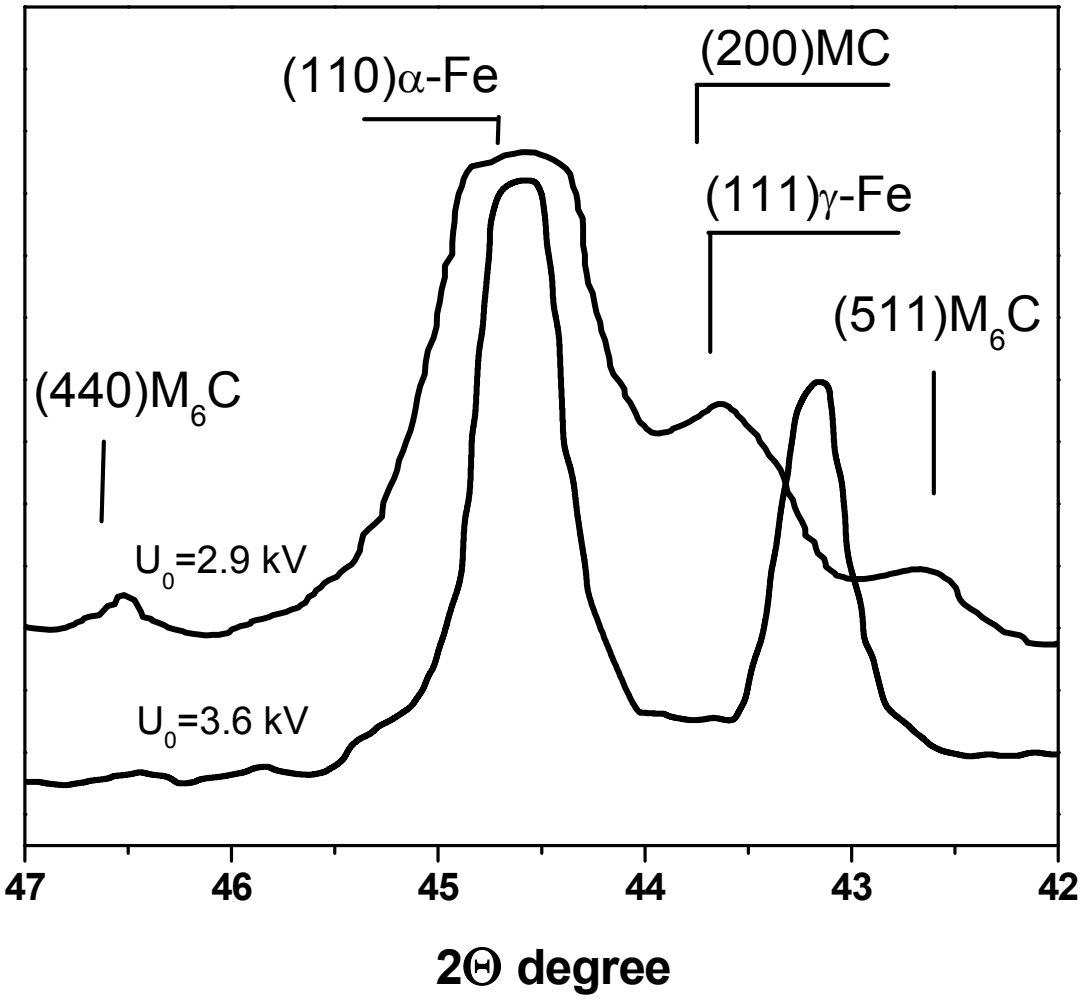
(110)α-Fe
(200)MC
(111)γ-Fe
(511)M6C
(440)M6C
U0=2.9 kV
U0=3.6 kV
47
46
45
44
43
42
2Θ degree

Fig. 2

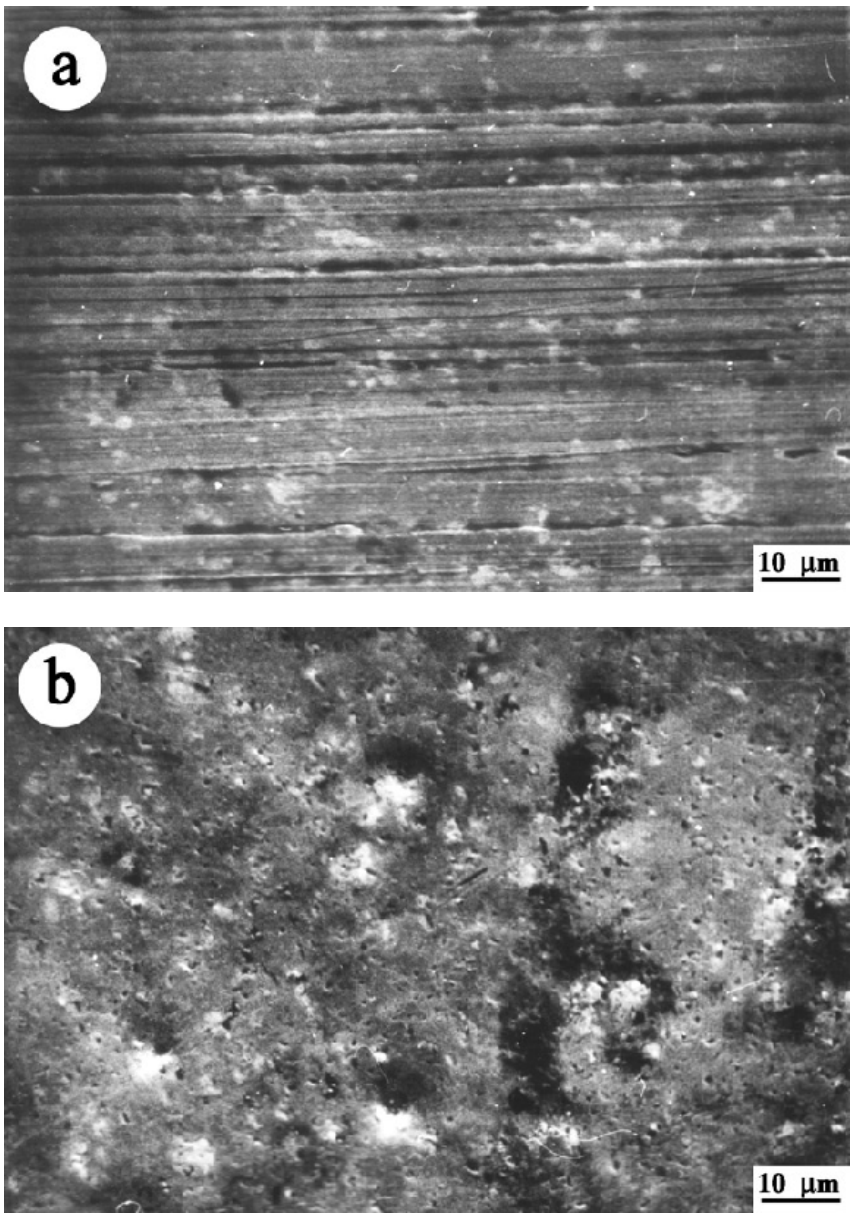

Fig. 3

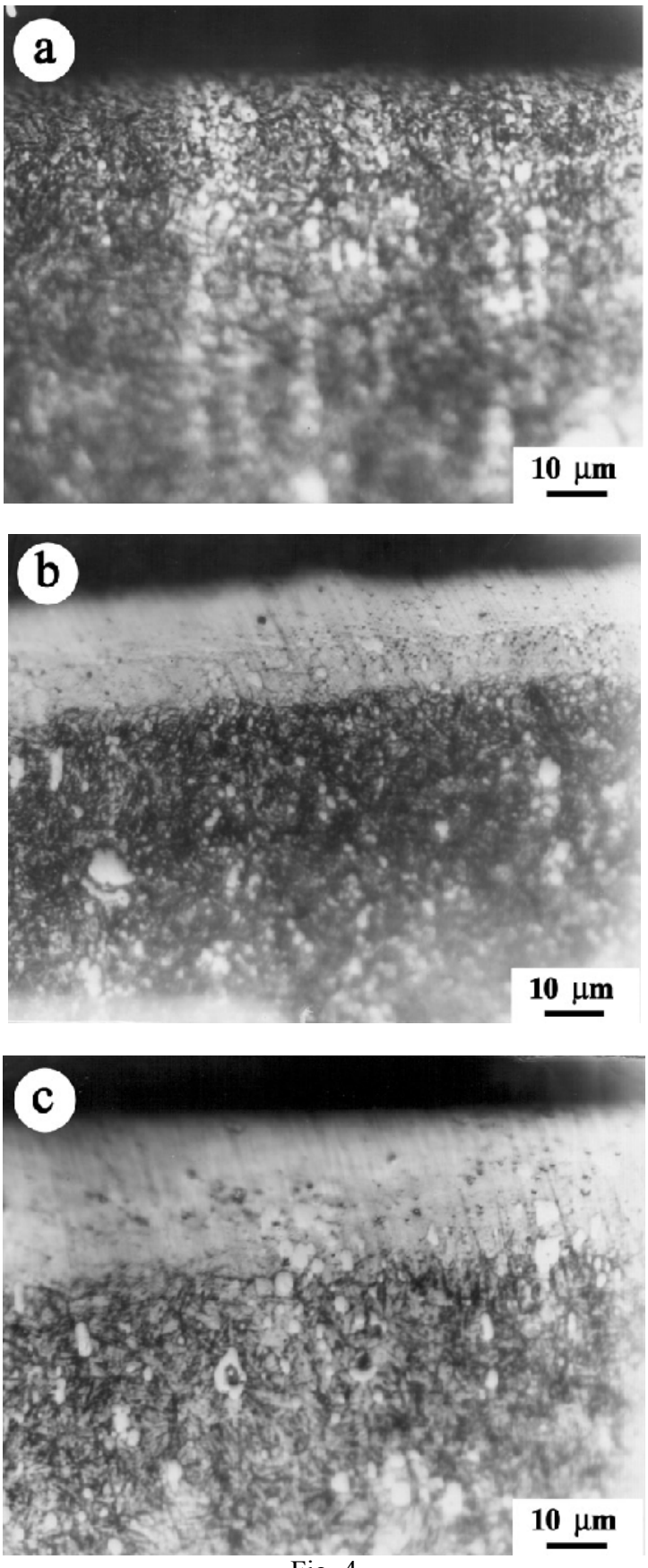

Fig. 4

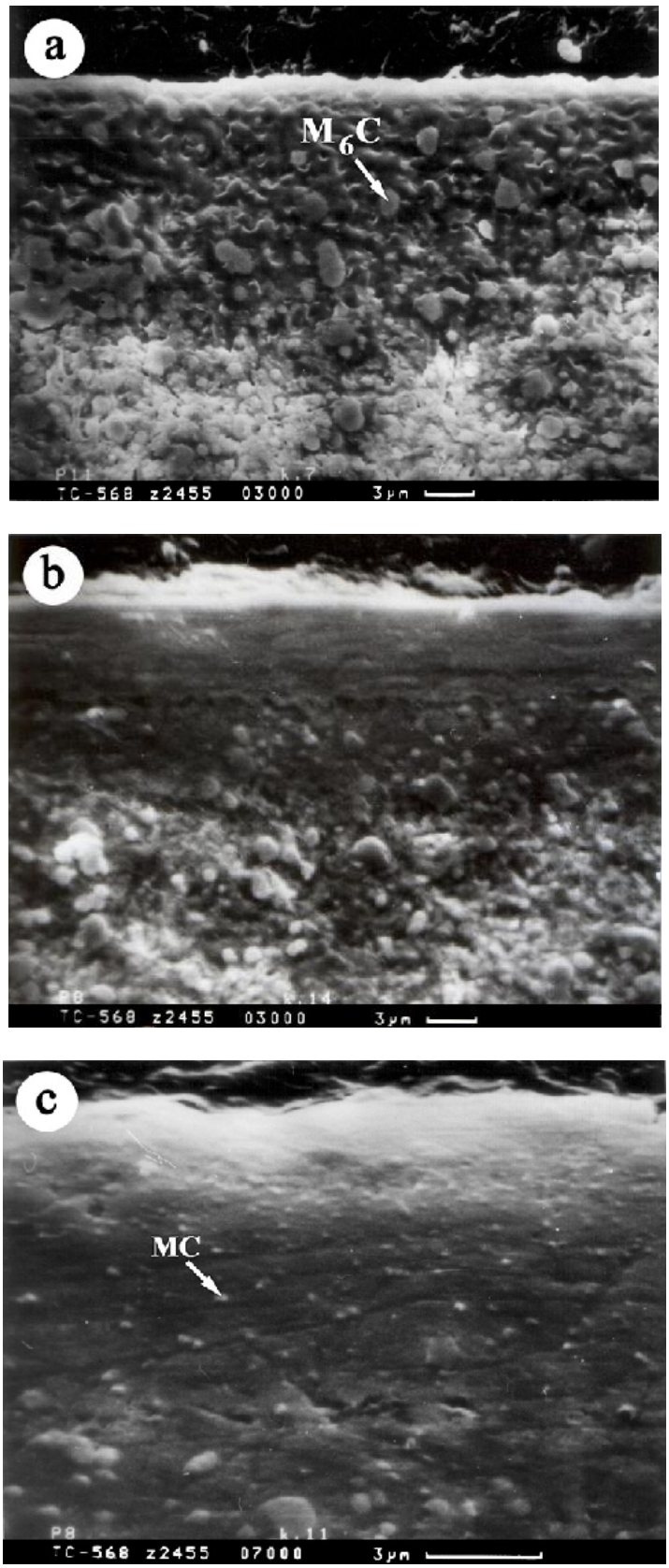
a
M6C
TC-568 z2455 03000 3μm
b
TC-568 z2455 03000 3μm
c
MC
TC-568 z2455 07000 3μm
Fig. 5

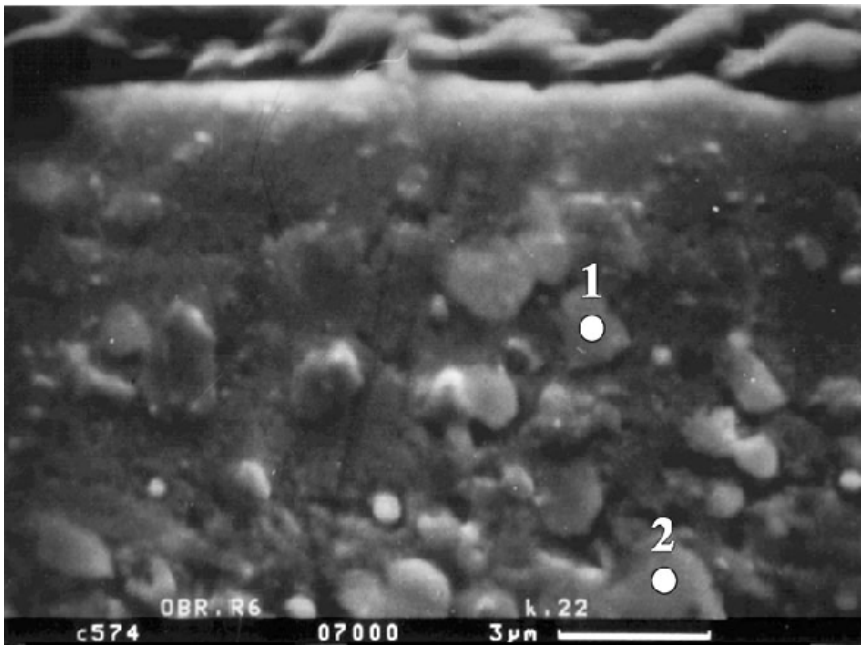

Fig. 6

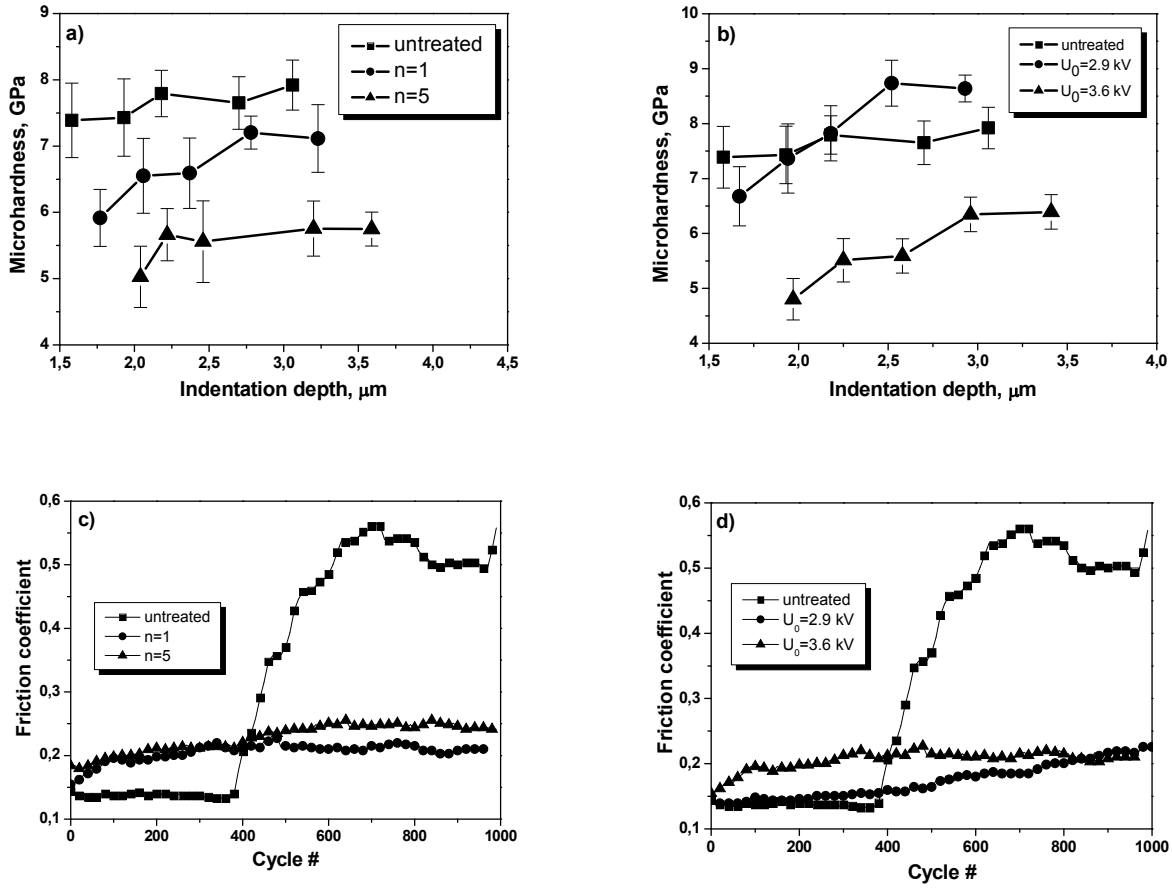
a)
untreated
n=1
n=5
Microhardness, GPa
Indentation depth, μm
b)
untreated
U0=2.9 kV
U0=3.6 kV
Microhardness, GPa
Indentation depth, μm
c)
untreated
n=1
n=5
Friction coefficient
Cycle #
d)
untreated
U0=2.9 kV
U0=3.6 kV
Friction coefficient
Cycle #

Fig. 7

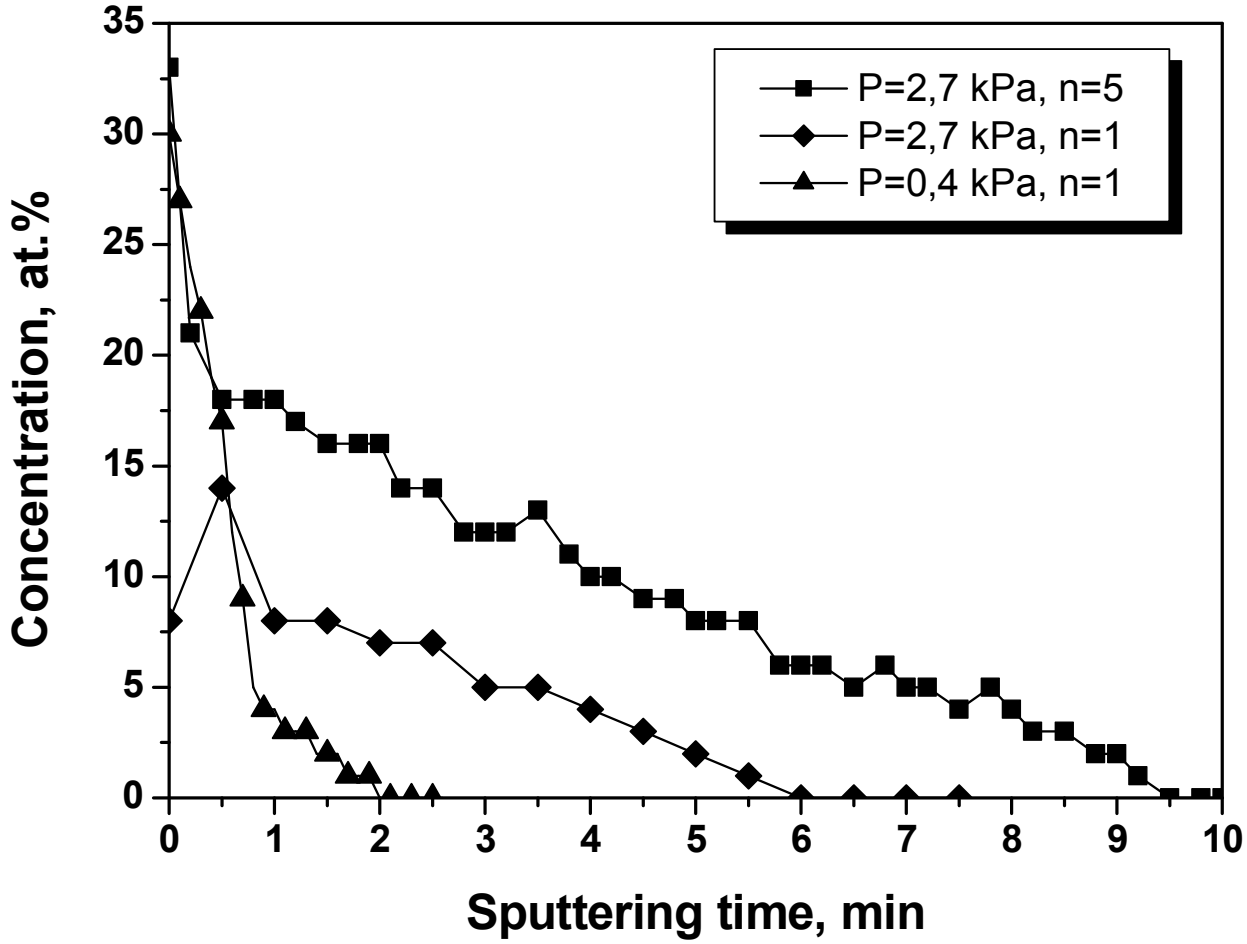
P=2,7 kPa, n=5
P=2,7 kPa, n=1
P=0,4 kPa, n=1
Concentration, at.%
Sputtering time, min
0
5
10
15
20
25
30
35
0
1
2
3
4
5
6
7
8
9
10

Fig. 8

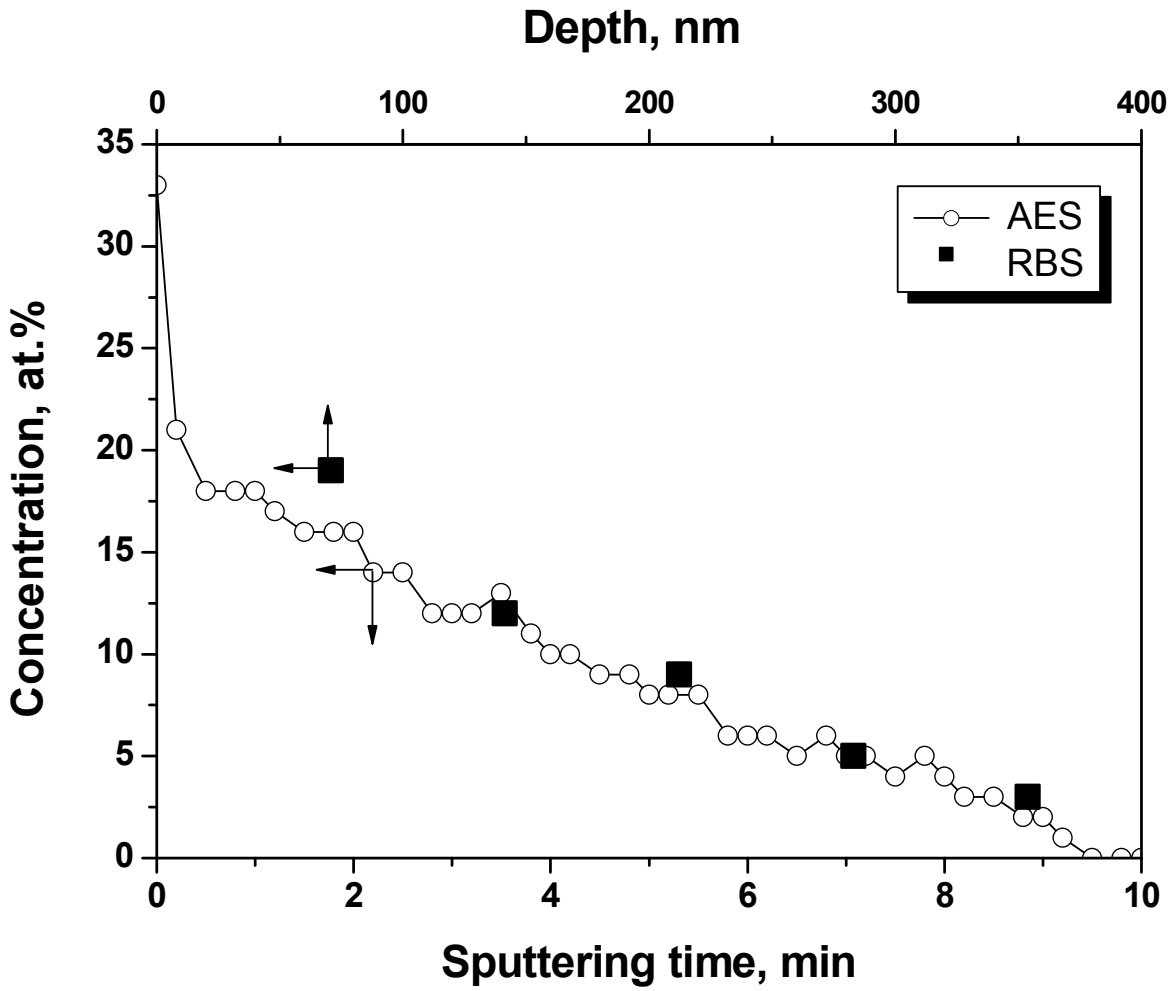
Depth, nm
0
100
200
300
400
35
30
25
20
15
10
5
0
Concentration, at.%
AES
RBS
0
2
4
6
8
10
Sputtering time, min

Fig. 9

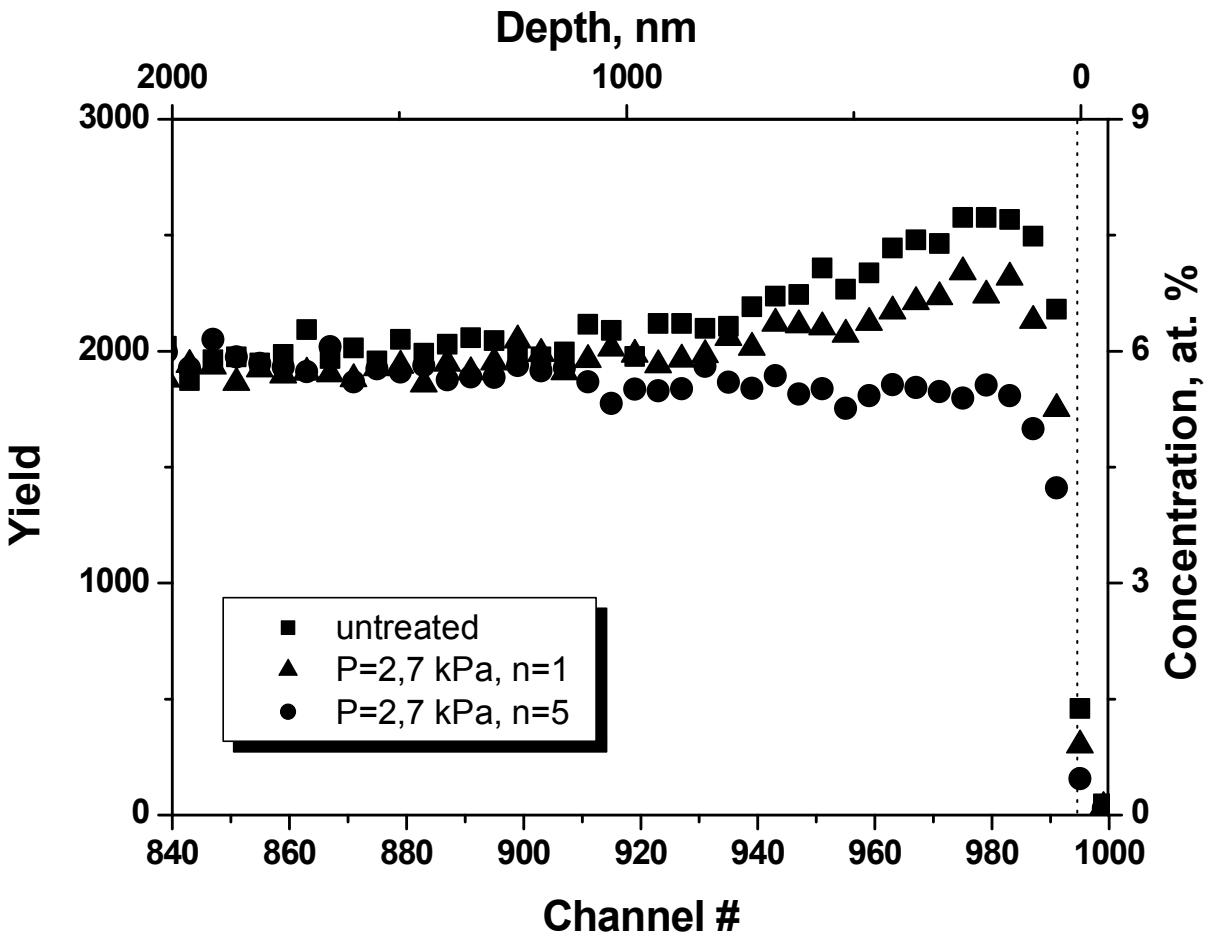
Depth, nm
2000
1000
0
3000
2000
1000
0
9
6
3
0
Yield
Concentration, at. %
untreated
P=2,7 kPa, n=1
P=2,7 kPa, n=5
840
860
880
900
920
940
960
980
1000
Channel #

Fig. 10

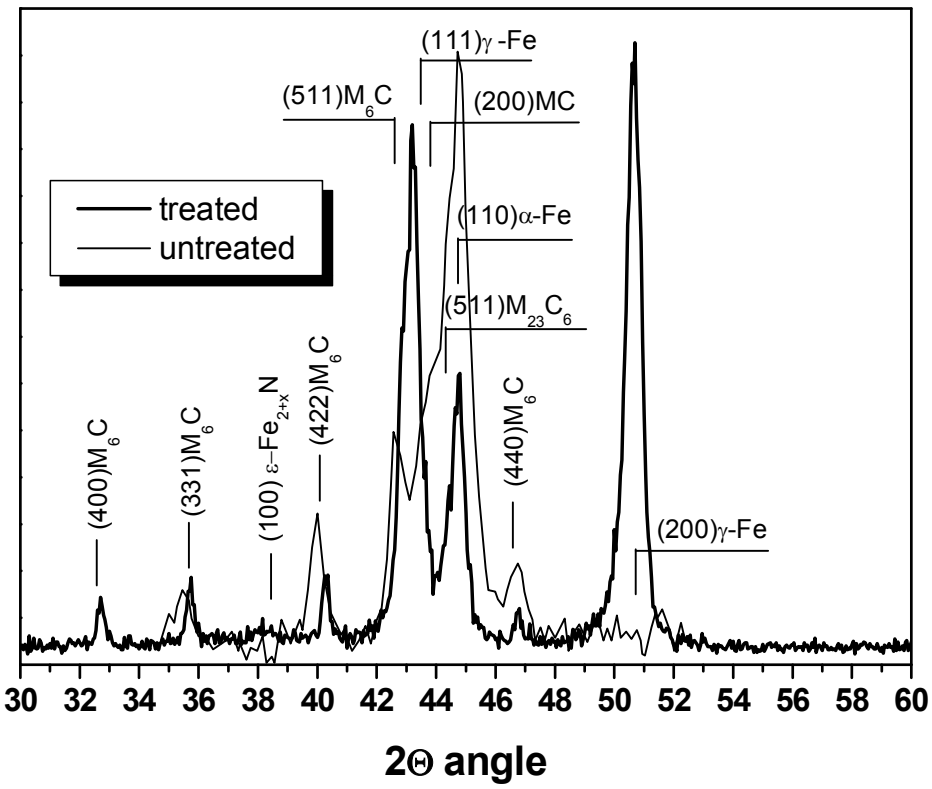
(111)γ -Fe
(511)M6C
(200)MC
treated
untreated
(110)α-Fe
(511)M23C6
(400)M6C
(331)M6C
(100) ε–Fe2+xN
(422)M6C
(440)M6C
(200)γ-Fe
30 32 34 36 38 40 42 44 46 48 50 52 54 56 58 60
2Θ angle

Fig. 11

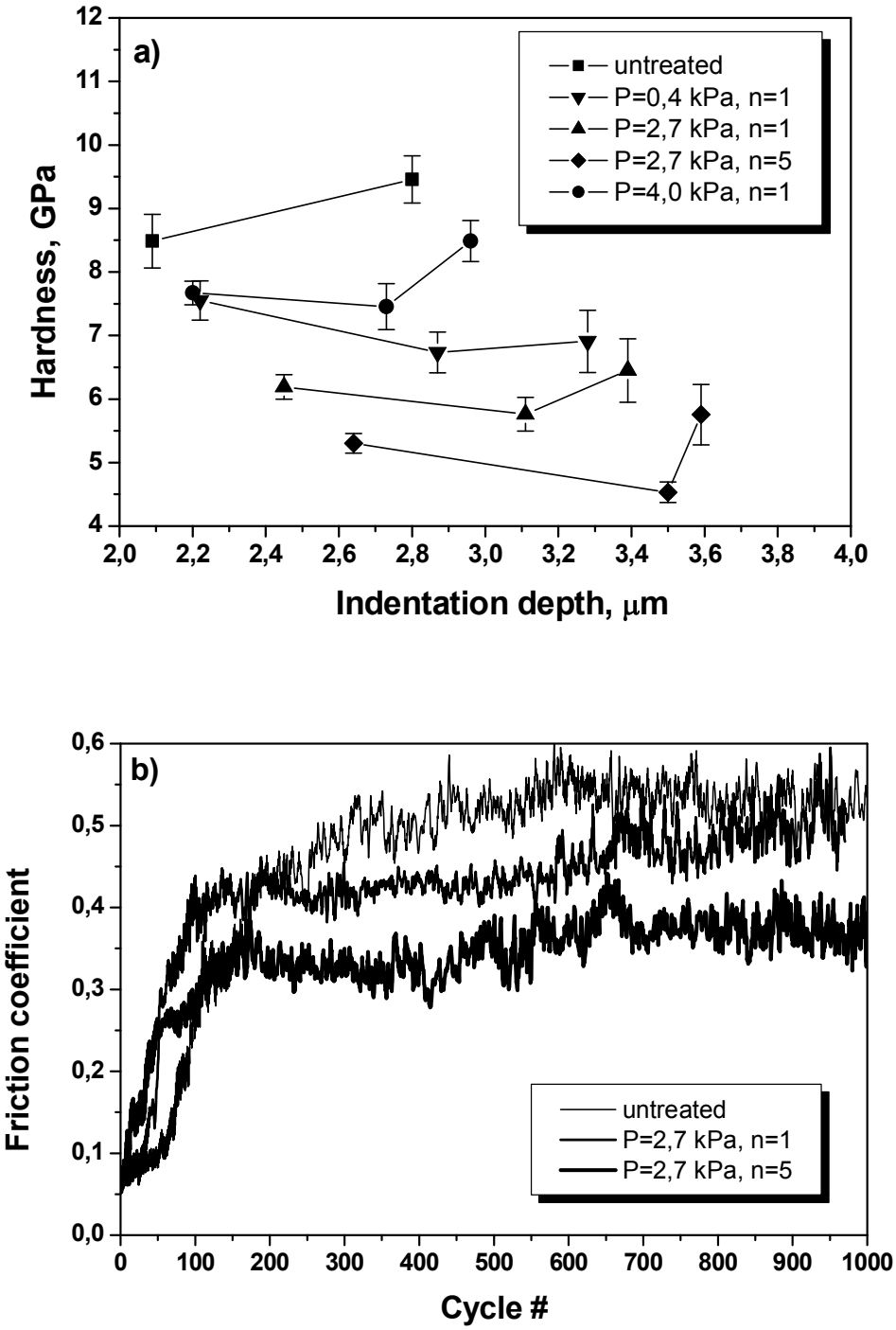
a)
untreated
P=0,4 kPa, n=1
P=2,7 kPa, n=1
P=2,7 kPa, n=5
P=4,0 kPa, n=1
Hardness, GPa
Indentation depth, μm
b)
untreated
P=2,7 kPa, n=1
P=2,7 kPa, n=5
Friction coefficient
Cycle #

Fig. 12